Accepted Article

Annual variations in GPS-measured vertical displacements near Upernavik Isstrøm (Greenland) and contributions from surface mass loading

Lin Liu[1], Shfaqat Abbas Khan[2], Tonie van Dam[3], Joseph Ho Yin Ma[1*], Michael Bevis[4]

[1] Earth System Science Programme, Faculty of Science, The Chinese University of Hong Kong, Hong Kong, China.

[2] DTU Space-National Space Institute, Technical University of Denmark, Department of Geodesy, Kgs. Lyngby, Denmark.

[3] Faculty of Science, Technology, and Communication, University of Luxembourg, Luxembourg City, Luxembourg.

[4] School of Earth Sciences, Ohio State University, Columbus, Ohio 43210, USA.

*Current address: Department of Civil and Environmental Engineering, Faculty of Engineering, National University of Singapore, Singapore.

Corresponding author: Lin Liu (liulin@cuhk.edu.hk)

Key Points:

- Atmospheric pressure loading contributes to half of the GPS vertical displacements at annual periods
- Annual verticals are sensitive to ice mass balance over 85% of the entire ice sheet
- Differential verticals between stations are useful to constrain ice mass changes within 120 km

This article has been accepted for publication and undergone full peer review but has not been through the copyediting, typesetting, pagination and proofreading process which may lead to differences between this version and the Version of Record. Please cite this article as doi: 10.1002/2016JB013494

© 2016 American Geophysical Union. All rights reserved.

Accepted Article

Abstract

In response to present-day ice mass loss on and near the Greenland Ice Sheet, steady crustal uplifts have been observed from the network of Global Positioning System (GPS) stations mounted on bedrock. In addition to the secular uplift trends, the GPS time series also show prominent annual variability. Here we examine the annual changes of the vertical displacements measured at two GPS stations (SRMP and UPVK) near Upernavik Isstrøm in western Greenland. We model elastic loading displacements due to various surface mass loading including three non-ice components: atmospheric pressure, ocean bottom pressure, continental water storage, and one ice component, i.e., surface mass balance (SMB). We find that the contribution from atmospheric pressure changes can explain 46% and 78% of the annual amplitude observed in the GPS verticals at SRMP and UPVK, respectively. We also show that removing the predicted loading displacements due to SMB adversely increases the annual variance of the GPS residuals. However, using the GPS data alone, we cannot identify the exact cause(s) of this discrepancy because the annual loading displacements are sensitive to the SMB changes from over 85% of the ice sheet area. Alternatively, by differencing vertical displacements between the two stations, we find a good agreement between the modeled differential SMB loading displacements and the GPS residuals after removing non-ice components. Our study highlights the necessity of correcting for non-ice loading contributions in the GPS measurements of crustal deformation to infer ice mass changes in Greenland at annual periods.

© 2016 American Geophysical Union. All rights reserved.

Accepted Article

1 Introduction

Since 2007, more than 50 continuous Global Positioning System (GPS) stations have been established around the Greenland Ice Sheet (GrIS) in a network called GNET (Figure 1a). These stations, mounted on bedrock, aim to measure the solid Earth's response to glacial mass changes on the ice sheet. Specifically, there are two geophysical signals of primary concern: the visco-elastic response of the Earth to glacial history over the past thousands of years in a global scale, or the glacio-isostatic adjustment (GIA), and the elastic response to present-day variations on and near the GrIS. Using GPS data at pre-GNET stations in Greenland, earlier studies used the observed uplift and subsidence to quantify both elastic and visco-elastic processes [e.g., *Wahr et al*., 2001; *Khan et al*., 2007; *Khan et al*., 2008; *Jiang et al*., 2010; *Khan et al*., 2016].

In a network-wide study, *Bevis et al.* [2012] reported steady uplift at all the GNET stations in the past few years, predominantly due to the ongoing ice mass loss. Several local-scale studies used uplift at individual stations to infer multi-year mass loss from nearby outlet glaciers [e.g., *Khan et al.*, 2010; *Nielsen et al*., 2012; *Bevan et al*., 2015]. For instance, Figure 1b shows time series of GPS vertical coordinates at two stations, both of which exhibit strong uplift trends. Such trends are caused by the secular mass loss from the nearby glaciers [*Nielsen et al*., 2012].

In addition to the secular uplift trends, the GNET GPS time series also show prominent annual variability [*Bevis et al.*, 2012]. The observed annual variability, if due to surface mass loading, must be purely elastic and synchronous with the surface mass changes. *Bevis et al.* [2012] argued that the annual cycle of displacement recorded by all GNET stations is driven by both seasonal cycles in ice mass and by seasonal cycles in air mass. We confirm this hypothesis by using two GNET stations to show that the maximum of the annual uplift cycle occurs roughly three months after the minimum of the annual ice mass cycle. We postulate

© 2016 American Geophysical Union. All rights reserved.

Accepted Article

that this phase offset arises because various surface mass components, including ice, atmosphere, and water (on land and in the ocean) would all contribute to the amplitude and phase of the annual crustal deformation. However, there has been a lack of assessment of the annual loading from these various sources at individual GNET stations, which hinders the detection and subsequent analysis of glacial mass variability at annual scales in the GPS coordinate time series. Mis-modeling of annual loading signals may also introduce uncertainties in the estimation of secular deformation trends [*Santamaría-Gómez and Memin*, 2015].

In this paper, we study the annual GPS vertical coordinate time series (hereafter referred to as 'GPS data') with the primary goal of separating the non-ice and ice loading sources by modeling the contributions from atmospheric pressure (ATM), ocean bottom pressure (OBP), and continental water storage (CWS). Here we only use two GPS stations near Upernavik Isstrøm on the western coast of Greenland. This local-scale study facilitates detailed analyses and comparisons of various loading contributions. A local perspective also allows us to ignore complications in the observations of uplift due to the significant spatial variability expected from different surface mass components on and near the ice sheet. Also, by taking the difference between these two nearby stations, we would eliminate some common errors in the GPS data.

The second goal of this paper is to assess the possibility of further distinguishing between crustal deformation driven by changes in surface mass balance (SMB) and by glacial dynamics through an SMB model. SMB is the difference between accumulation processes (such as snowfall) and ablation processes (such as surface melting that becomes runoff). Accumulation and runoff are well known to vary strongly at annual and inter-annual time scales, largely driven by changes in weather conditions [*Abdalati and Steffen*, 2001; *Hanna et al.*, 2011]. Glacial dynamics refers to the flow of ice from the interior of the ice sheet

© 2016 American Geophysical Union. All rights reserved.

outwards through outlet and land-terminating glaciers. Numerous studies have reported marked seasonal changes in ice dynamics at many major outlet glaciers and also near the margin of the ice sheet [e.g., *Joughin et al*., 2008; *Sole et al*., 2011]. These seasonal changes of ice motions redistribute ice mass and alter total mass balance at outlet glaciers.

2 Study Area and Method

2.1 Upernavik Isstrøm and the nearby GPS stations

Upernavik Isstrøm consists of four glaciers, denoted as Glaciers 1–4 proceeding from north to south (Figure 1c). In 2011, the GPS station SRMP (54.3937W, 72.9107N) was located only 1.5 km west of the Glacier 2's frontal position, whereas UPVK (56.1280W, 72.7883N) is on an island 65 km further west of the glaciers.

Previous studies have focused on quantifying multi-year changes of this glacier complex [*Nielsen et al*., 2012; *Khan et al*., 2013]. They have estimated an ice mass loss rate of 6.7 Gt/year for the period of 2005–2010, with dynamic changes accounting for 80% of the total mass loss and the remaining 20% due to negative SMB. However, the four glaciers have exhibited asynchronous dynamical changes in the past decade; significant retreat and speedup have been observed at Glacier 1 with only moderate or little change at the other three glaciers [*Nielsen et al*., 2012; *Andresen et al*., 2014; *Larsen et al*., 2016].

Accepted Article

© 2016 American Geophysical Union. All rights reserved.

Accepted Article

2.2 GPS data analysis

We process the GPS data using conventional methods detailed in *Khan et al*. [2010]. We use the GIPSY-OASIS v6.3 software package developed at the Jet Propulsion Laboratory (JPL). We use the JPL final orbit products and take the satellite antenna phase center offsets into account (antenna phase center file igs08_1869.atx). The atmospheric delay parameters are calculated from the global VMF1FGRID grid files at 6-hour intervals [*Boehm et al*., 2006; *Kouba*, 2008]. We apply the second order ionospheric correction. At the operational level of GPS data analysis, we remove the ocean tidal loading (OTL) displacements calculated using the online Automatic Loading Provider [*Scherneck and Bos*, 2002], applied to the FES2004 ocean tide model. The OTL displacements are in a reference frame fixed to the center of mass (CM). We estimate uncertainties in the daily GPS positioning solutions by accounting for temporally-correlated errors as a combination of Gaussian and flicker noise [*Williams et al*., 2004; *Khan et al*., 2010]. We use an elevation-dependent weighting function (sine of elevation angle) in the error estimation. We obtain time series of daily positioning solutions and their errors in the local east, north, and up directions in the IGS08 frame [*Altamimi et al*., 2012]. In this realization of the International Terrestrial Reference Frame, the frame origin is in the center of surface figure (CF) at annual time scales [*Dong et al*., 2003]. The UPVK antenna was replaced on September 16 2008. We estimate and correct for an offset on this day at this station. For the sake of visual clarity, all the time series figures presented in this paper are resampled to weekly intervals.

Because of our focus on the annual signal, we only analyze and interpret the detrended GPS data. We restrict our analysis to the GPS vertical coordinate time series as the annual amplitudes in these data are about one order of magnitude larger than in the horizontal coordinates (more in Section 3.1). Using least-squares estimation weighted with the GPS positioning errors, we fitted and removed a linear trend from each GPS time series. Because

© 2016 American Geophysical Union. All rights reserved.

Accepted Article

we have removed the linear trends, any secular geophysical contributions (such as GIA and tectonic motion) or errors (such as reference frame drift) have also been removed and are thus not considered here.

2.3 Modeling displacements due to surface loading

To quantify the glaciological contributions to the annual vertical coordinate signal from the two GPS stations, we must model and remove other non-ice loading contributions. Given any grid of surface mass changes, we use the elastic loading Green's functions calculated based on the PREM Earth model with continental crust to estimate the displacement response at the two GPS stations [*Dziewonski and Anderson*, 1981; *Jentzsch*, 1997]. Table 1 summarizes the source models we use to quantify surface mass variations, which are described in detail below. The modeled loading displacements are in the frame fixed to the center of mass of the solid Earth (CE), which is close to the CF [*Blewitt*, 2003]. For simplicity, we ignore the difference between these two reference frames (which only introduce differences of up to 0.6% in the modeled time series) and do not transform the loading displacements into the CF. All the loading displacement time series are resampled to match the daily GPS data.

To derive the surface deformation from atmospheric mass variability we use the surface pressure provided by the National Center for Environmental Prediction (NCEP) reanalysis data [*Kalnay et al.*, 1996]. This dataset is provided as a global grid with a spacing of 2.5° by 2.5° and a temporal sampling of 6 hours. Because we are only interested in relative temporal changes, we remove a thirty-year (1980–2010) mean of atmospheric pressure from each six-hour grid. Finally, we assume the oceans respond to the atmospheric pressure changes as an inverted barometer (IB) and introduce a globally uniform pressure change at the ocean

© 2016 American Geophysical Union. All rights reserved.

Accepted Article

bottom to conserve ocean mass [*van Dam and Wahr*, 1987]. For simplicity, in the remainder of this paper, we refer to the combined loading effects due to atmospheric pressure and IB ocean bottom pressure as the atmospheric pressure (ATM) loading.

We use the "Estimating the Circulation and Climate of the Ocean" (ECCO) dataset to quantify the non-IB ocean bottom pressure changes, referred to as OBP in the remainder of this paper. The version used is JPL's Kalman filter (kf66b) series, which assimilates altimetric heights, Expendable Bathythermographs (XBT) profiles, and other in situ ocean data [*Fukumori*, 2002; *Kim et al*., 2007]. The model used is the parallel version of the primitive equation Massachusetts Institute of Technology ocean global circulation model (MITgcm). The data cover the area from 80° S to 80° N. The horizontal grid spacing is 1° over most of the globe except within a band of 20° around the equator. The meridional grid spacing is gradually reduced to 0.3° within 10° of the equator. The ECCO OBP data are provided at 12-hour intervals. We note that oceanographic data have poor coverage in the Labrador Sea (southwest off Greenland), which may affect the accuracy of ECCO OBP data.

We use the Noah land hydrology model (version 2.7.1) in the Global Land Data Assimilation System (GLDAS) to quantify continental water mass changes at monthly intervals [*Rodell et al*., 2004, obtained from http://grace.jpl.nasa.gov]. The global, 1° by 1° product provides a sum of water stored as soil moisture, snow, canopy, but not including groundwater or the water storage changes in rivers or lakes. It also excludes water storage estimates from the Greenland Ice Sheet and permafrost areas.

To further partition glacial mass changes into SMB and dynamics components, we model loading from SMB using the climate simulation from the Regional Atmospheric Climate Model version 2.3 (RACMO2.3) [*Noël et al*., 2015]. The monthly SMB fields from 1958 to 2014 are provided on a grid of about 11 km by 11 km. We use the same ice mask as prescribed in RACMO2.3, which is on the same grid as the SMB fields. Following *van den*

© 2016 American Geophysical Union. All rights reserved.

Accepted Article

Broeke et al. [2009], we remove the 1961–1990 mean from the monthly fields, then integrate them over time and obtain a time series of mass balance for our study period of 2007.5 to 2014.7. The choice of the reference period only influences the secular trend but will have no impact on our detrended time series.

3 Results

3.1 GPS solutions and modeled loading displacements

The detrended GPS time series at SRMP shows a prominent annual signal over the entire seven years (Figure 2a). Further, we observe a strong peak at the annual period in the power spectrum of the GPS data (see the Figure 2b periodogram). In addition to the annual changes, the GPS time series is also characterized by quasi 4-year as well as moderate semi-annual and bi-annual cycles (Figures 2a and 2b). In comparison, the GPS time series at UPVK exhibits similar annual variability but is slightly reduced in amplitude (Figures 2c and 2d). The annual signal weakened between 2007.5 and 2011.5 and became more pronounced afterward. The UPVK periodogram also shows peaks at semi-annual, bi-annual, and quasi-4-year periods (Figure 2d).

To account for these periodicities, we model the detrended GPS time series of vertical coordinates H as a Fourier series composed of four harmonics:

$$H(t) = \sum_{i=1}^{4} A_i \cos\left[\frac{2\pi}{T_i}(t - t_0^i)\right], (1)$$

where t is time (units: days); the four periods ($T_{i,\, i=1\text{–}4}$) are one solar year (365.24 days), half, two, and four solar years; A_i and t_0^i are amplitude and phase for the i^{th} period. Using this model to fit the detrended GPS data, we obtain the best-fit annual amplitudes as 4.8 mm and 2.3 mm at SRMP and UPVK, respectively (Table 2). The annual cycles at these two stations peak around December 1 and January 1, respectively.

© 2016 American Geophysical Union. All rights reserved.

Accepted Article

We also fit the GPS horizontal time series with the same harmonic model but find small annual amplitudes. The best-fit annual amplitudes are only 0.40 mm (east-west components at SRMP), 0.68 mm (north-south components at SRMP north), 0.23 mm (east-west components at UPVK), and 0.86 mm (north-south components at UPVK), which are 3 to 10 times smaller than the annual vertical amplitudes (see Figure S1 of the Supporting Information). Horizontal displacements may help in loading studies by providing more constraints, especially on the azimuthal directions of surface mass changes [e.g., *Grapenthin et al.*, 2006; *Wahr et al.*, 2013]. However, further analysis and interpretation of horizontal displacements are beyond the scope of this study.

The time series of modeled vertical loading displacements due to various surface mass changes show strong annual variability, moderate semi-annual variability, and no significant variability at other periods (Figures 3 and 4). We therefore only include the annual and semi-annual terms in the time series model of our modeled loading displacements. At SRMP and UPVK, the modeled ATM loading displacements have amplitudes of 3.4 mm and 2.8 mm, respectively. The maximum for both stations occurs around January 1, similar to the annual phase of the GPS observations. Loading displacements due to changes in CWS are nearly identical at the two stations, dominated by an annual cycle with amplitudes of only 1.1 mm, peaking around September 15 (Figures 3b, 3e, 4b, 4e). This is expected because the CWS over the ice sheet are eliminated so that the annual signal is driven by mass changes in the far field. The amplitude of the annual loading displacements due to OBP changes is smaller than 0.2 mm, almost negligible (Figures 3b and 4b).

© 2016 American Geophysical Union. All rights reserved.

Accepted Article

The SMB loading displacements are characterized by strong annual, moderate semi-annual, and weak bi-annual cycles (Figures 3c, 3f, 4c, 4f). At SRMP, the annual amplitude of the SMB loading displacements is 4.3 mm, larger than that of the ATM loading. At UPVK, which is further away from the ice sheet, the annual amplitude of the SMB loading displacements is 2.0 mm, smaller than that of the ATM loading. Including both annual and semi-annual cycles, the overall SMB loading displacements peak around September 1, the end of summer melting season (Figures 3c and 4c).

Inter-annual variations are also evident in the SMB loading displacement time series. For instance, the net SMB uplift at SRMP during JJA in 2012 was ~ 14 mm, or 4 mm larger than the mean net uplift (~ 10 mm) during the same summer months in 2008 to 2011 (Figure 3c). In contrast, the net SMB maxima during JJA in 2013 and 2014 were ~ 6 mm and ~ 8 mm, respectively, smaller than the 2008–2011 mean.

3.2 GPS residuals after removing modeled loading displacements

We remove the modeled displacements from the GPS vertical displacements in the following sequential steps: (1) the ATM loading displacements, (2) the loading displacements due to OBP and CWS combined, and (3) the SMB loading displacements. Figures 5 and 6 show the residuals obtained after each step.

We evaluate the residuals in two ways. First, we calculate the amplitude and phase of the best-fit annual to the residuals obtained after each correction step (Table 3). After removing the modeled atmospheric loading displacements, the annual amplitudes decrease by 2.2 mm (46%) and 1.8 mm (78%) from the original GPS amplitudes at SRMP and UPVK, respectively (also compare Figure 5b with 5a and Figure 6b with 6a). After the further removal of the modeled displacements due to OBP and CWS loading, the annual amplitude

© 2016 American Geophysical Union. All rights reserved.

Accepted Article

decreases by 0.8 mm to 1.8 mm at SRMP (also Figure 5c), but instead increases by 0.7 mm to 1.2 mm at UPVK (also Figure 6c). Taken together, removing all the non-ice components reduces the annual amplitudes by 3 mm (63%) at SRMP and 1.1 mm (48%) at UPVK. Finally, and unexpectedly, after the removal of the modeled SMB loading displacements, the annual amplitudes increase by 0.9 mm (50%) and 2 mm (167%) from the previous step at SRMP and UPVK, respectively (also see Figures 5d and 6d). Comparing Figure 5d with 5c, we also note a phase shift from the 309th day of year for the residuals after the removal of the non-ice components to the 85th day of year after the further removal of the SMB components (Table 3). In contrast, the phase shift between these two steps is negligible at UPVK (Figures 6c, 6d, and Table 3).

We also calculate the weighted root-mean-squares (WRMS) of the residuals and the corresponding ratio of reduced WRMS after removing each loading component. We decompose each of the residuals time series into long-period and short-period components, separated by 0.5 years. Table 4 lists the calculated ration of WRMS reduction from the original GPS vertical time series. Because of our focus on the annual signatures, here we only summarize the results using the long-period components. At SRMP, ATM loading can explain 26% of the WRMS for the long-period components, followed by the SMB (24%), the CWS (4%), and negligibly but reversely from the OBP (-0.6%). Overall, these modeled loading displacements account for 41% of the WRMS at the long periods. At UPVK, the ATM loading reduces the WRMS for the long-period components by 21%. The CWS and SMB instead increase the WRMS by 5% and 4%, respectively. Overall, these modeled loading displacements unfavorably increase the WRMS at the long periods by 3%.

© 2016 American Geophysical Union. All rights reserved.

Accepted Article

In summary, the combined facts that the removal of SMB loading (1) increases the annual amplitudes of the GPS residuals at both stations, (2) shifts the annual phase by 224 days at SRMP, and (3) increases the WRMS at UPVK for the long-period components, indicate that the modeled SMB loading increases the annual variance of the GPS residuals after the removal of the non-ice loading. This contradicts to our expectation that the SMB loading should partly explain the GPS residuals. The residuals obtained after the further removal of the SMB loading (i.e. Figures 5d and 6d) are questionable and cannot be used to interpret the contribution from the glacial dynamics to the total ice mass changes.

4 Discussion

4.1 Performance of modeled surface mass loading displacements

We use alternative elastic Earth models to assess the uncertainties of the modeled SMB loading displacements. We perform the same elastic loading calculation as described in Section 2.3, but using the following six one-dimensional spherical models: (1) an older, poorly constrained Gutenberg-Bullen A (G-B) model, (2) the PREM model with oceanic crust, (3) the PREM model with the crustal structure as modeled in Crust 2.0 [*Laske et al*., 2012] with hard sediments, (4) the PREM model with the crustal structure as modeled in Crust 2.0 with soft sediments, (5) the ak135 model, and (6) the iasp91 model. The elastic loading Green's functions for models (1) and (2) are provided in *Farrel* [1972] and *Jentzsch* [1997], respectively; the others are provided in *Wang et al*., [2012]. Together with the PREM continental-crust model that we have adopted as a baseline, we analyze the ensemble of these seven sets of modeled vertical displacements due to the same SMB loading. We find that these Earth models give similar displacements (Supporting Information Figure S2). Take the monthly displacement values at SRMP as an example: our calculations show that the standard deviation of the ensemble is less than 0.43 mm; the maximum difference between the

© 2016 American Geophysical Union. All rights reserved.

Accepted Article

displacements from the baseline model and the ensemble mean is only 0.2 mm. The best-fit annual amplitude of the ensemble mean is 4.1 mm with a 5% variance. This, again, is very close to the best-fit annual amplitude of 4.2 mm based on the baseline model. Among all the Earth models considered, the PREM oceanic-crust model gives the largest differences from the baseline model with an annual amplitude that is 0.4 mm (10%) smaller. These similarities are because (1) the loading Green's functions of these spherical Earth models differ mostly in the near field (shorter than 100 km from the loads) [*Wang et al.*, 2012] and (2) as will be shown later in this section and Figures 7 and 8, a significant portion of the SMB loading fields is located in the far field and contributes to the loading displacements at the annual period. We note that the analysis described above does not quantify the effects of lateral variations of crustal structure on the modeled loading displacements. However, according to *Dill et al.* [2005], such effects cause a maximum of 10% in the annual vertical displacements over western Greenland.

We also assess the variances in the SMB models using four other sets of regional atmospheric climate model outputs. These alternative models include the earlier RACMO version 2.1 model [*van den Broeke et al.*, 2009; *van Angelen et al.*, 2012] and the MAR v3.5.2 with three different forcing models (ERA-Interim, NCEP-NCARv1, 20CRv2) [*Fettweis et al.*, 2013]. Our calculated loading displacements based on these five models have similar annual cycles (Supporting Information Figure S3). For instance, the ensemble mean of the annual amplitude is 4.1 mm at SRMP with a standard deviation of 0.2 mm. This is very similar to the 4.2 mm obtained using the RACMO2.3 outputs.

© 2016 American Geophysical Union. All rights reserved.

Accepted Article

In fact, the annual SMB vertical loading displacements at the two GPS stations are attributed to surface ice mass changes over large portions of the GrIS. We first use the RACOM2.3 outputs estimate the annual SMB changes over the entire model domain during our study period. Figure 7a shows the best-fit annual amplitude. We then calculate the total contribution to the annual SMB loading displacement from each of the following units: the six major drainage basins of the GrIS (based on Rignot et al., 2011), glaciers around the periphery of Greenland (based on the Randolph Glacier Inventory 5.0, http://www.glims.org/RGI/), ice fields outside Greenland (including the Canadian Arctic, Svalbard, Jan Mayen, and Iceland). Figure 7b summarizes their contributions. At SRMP, 73% of the annual loading displacements originate from the northwest drainage basin, followed by much smaller contributions from outside Greenland (8%), the central-west (7%), southwest (5%), and southeast (3%) drainage basins. At UPVK, the order of contribution is similar to that of the SRMP: 48% is from the northwest drainage basin, followed by outside Greenland (16%), the central-west (13%), southwest (9%), and southeast (5%) drainage basins. The contributions from the remaining units are small at both stations. Figure 8 shows the cumulative contribution to the annual SMB loading displacement from surface ice sources located at different distances. At SRMP, ~ 70% of the annual loading displacements originate from surface ice mass variations within ~ 100 km. However, the remaining 30% is attributed to surface ice mass within 1200 km radius (~85% of the entire ice sheet area and outside Greenland). At UPVK, which is located further away from the ice sheet, 50% of its annual SMB loading displacements origin from surface ice mass within 200 km.

© 2016 American Geophysical Union. All rights reserved.

Accepted Article

4.2 Differential vertical displacements between the two stations

In the GPS data analysis, a few mismodeled or unmodeled factors may also result in errors with annual signature and thus affect our interpretation. As summarized in *Dong et al*. [2002], some factors are local at individual stations such as multi-path and snow cover on the receiver antenna; and some factors are regional or global, such as the reference frame, mismodeled wet tropospheric delay, errors in orbital modeling. Even though significant improvements have been made in the GPS analysis in the past decade, some of these errors are not well understood or corrected and thus may remain.

Here we examine the differences between SRMP and UPVK, in which we have eliminated the common errors in the GPS data. The station difference still shows a strong annual variability with an amplitude of 3.1 mm (Figures 9a and 9b, Table 5). However, we also have removed any common geophysical signals. For instance, if the 4.8 mm annual amplitude at SRMP is entirely of geophysical origins, we have removed 1.7 mm (35%) of the signals by taking the station difference.

To further quantify what may have been removed, we take the difference of the modeled surface mass loading displacements between the two stations. Figure 10 shows these differential time series. Table 5 lists the annual amplitudes of the differential loading displacements: 0.6 mm for the ATM loading, nearly zero (0.1 mm) for the OBP, zero for the CWS, and 2.2 mm for the SMB loading. Compared with the Table 2 results for SRMP, we have removed 2.8 mm (82%) of the ATM loading, 2.1 mm (49%) of the SMB loading, and nearly the entire of the OBP and CWS.

.

© 2016 American Geophysical Union. All rights reserved.

Accepted Article

After the station differencing, the SMB signals become the most dominant component among all the modeled surface mass displacements at annual periods. We conduct a similar sensitivity analysis to the one described in Section 4.1 but for the differential SMB loading displacements. Compared with the individual sensitivity curves shown in Figure 8, the differential sensitivity (Figure 11) reveals a significant contribution from nearby surface ice: SMB changes within 40 km from SRMP contribute to about 80% of the differential SMB-loading displacements at the annual period. There is little sensitivity to SMB beyond 120 km from SRMP. This is also confirmed by our estimated contributions from different units to the annual differential SMB uplift (summarized in Figure 7b). As expected, the northwest drainage basin is the dominant contributor (84%), followed by the peripheral glaciers (15%), and merely 1% from the central-west drainage basin. Contributions from the other units are negligible.

Lastly, we remove modeled differential loading displacements from the measured differential GPS in sequential steps as described in Section 3.2. Tables 6 and 7 list the best-fit annual amplitudes/phases and ratios of WRMS reduction. We observe that the differential SMB match with the differential GPS the best. Removing the differential SMB can reduce the WRMS of the long-period components by 47%. Removing all the modeled differential loading displacements, the annual amplitude is reduced to 0.7 mm (or 23% of the differential GPS before the corrections) and the WRMS reduction of the long-period components is 55%. Figures 9c and 9d show the time series and periodogram of the residuals after removing all the modeled loading components. From these figures, it is evident that the models significantly reduce the annual amplitude and data variance.

© 2016 American Geophysical Union. All rights reserved.

Accepted Article

Although the differential SMB loading displacements match the differential GPS residuals well, we cannot uniquely confirm the accuracy of the SMB model in the near field of the GPS stations. This is because by taking station difference, we have removed 2.1 mm of common SMB loading signals. These common SMB loading signals originate from all the ice fields. We cannot rule out the possibility that the deficits in the SMB model (if any) might be localized in near field. Theoretically, an extreme case that an SMB bias is at a point location, which may cause a similar bias in the annual loading at both stations. However, taking a station difference would have removed such common bias and still gives good residual results as presented above.

4.3 Unmodeled GPS draconitic errors and surface mass loading displacements

In addition to annual periodicity, many GPS position time series have a 351.2-day harmonic at the GPS draconitic year as well as its higher harmonics [*Ray et al*., 2008; *Amiri-Simkooei*, 2013]. However, we have chosen to exclude the draconitic harmonics in the Fourier series model (equation 1) for two reasons. First, neither of the 8-year GPS time series at SRMP or UPVK shows a peak at 351.2 days (Figures 2a and 2c). Second, we find that including the draconitic harmonics in the least-squares fitting using the daily GPS data results in a strong negative correlation between the draconitic and annual cycles. Such a trade-off indicates an over-fitting problem and that the GPS data used in this study are not able to separate the draconitic and annual cycles. However, because the draconitic signals are so close to a pure annual, they may still contribute to the annual amplitude and phase in the GPS data. Quantifying such error will become feasible as the GPS time series are getting longer.

The CWS loading model based on GLDAS excludes groundwater, river and lakes, and permafrost. The unmodeled vertical displacements due to these water mass changes are expected to have annual variability, but their amplitudes are smaller than our modeled CWS loading. Depending on the annual phases of these mass sources, they may not add

© 2016 American Geophysical Union. All rights reserved.

Accepted Article

constructively. Including these terms may help to reduce the overestimation of CWS loading at UPVK.

5 Conclusions

To quantitatively interpret the annual changes of the vertical displacements measured at two GNET GPS stations, 65 km apart near Upernavik Isstrøm, we present a systematic study to model and correct various surface mass loading components. Among all the non-ice mass changes, atmospheric pressure changes introduce the largest annual changes at both stations, followed by continental water storage, with negligible contributions from ocean bottom pressure. Removing the non-ice loading contributions can reduce the annual amplitudes by at least 50%. This suggests the need for applying this correction before using annual GPS signals to infer ice mass changes.

Our modeled SMB loading based on RACMO2.3 increases the annual variance of the GPS residuals, which makes it difficult to estimate contributions from the annual variability of glacial dynamics to the total ice mass balance. Our analysis reveals that GPS verticals at individual stations are sensitive to annual ice mass changes over 85% of the entire ice sheet and outside Greenland. This long-distance sensitivity indicates the non-uniqueness and therefore the difficulty of using GPS data alone to detect possible defects in the SMB model, especially their locations.

Alternatively, by taking station difference, we find a good match between the modeled SMB loading and the estimated GPS vertical displacements. Our forward modeling shows the sensitivity of the differential loading displacements to local SMB changes. This suggests that differential displacements measured at a local GPS network can potentially help to place constraints on estimates of annual glacial mass balance obtained, for instance, from glaciological estimates.

© 2016 American Geophysical Union. All rights reserved.

Acknowledgment and Data

The GLDAS continental water products were produced by the Goddard Earth Sciences Data and Information Services Center and obtained from the GRACE-Tellus website (http://grace.jpl.nasa.gov). We thank the associate editor, R. Grapenthin, and two anonymous reviewers for their insightful comments, which help to improve the quality of this paper. We thank M. van den Broeke for providing RACMO v2.1 and v2.3 SMB fields over Greenland. Work at the Chinese University of Hong Kong was supported by Hong Kong Research Grants Council Grant CUHK24300414. S.A.K. was funded in part by Carlsbergfondet (grant CF14-0145) and the Danish Council for Independent Research (grant DFF-4181-00126). Raw GPS data are available from the UNAVCO Facility with support from the National Science Foundation (NSF) and National Aeronautics and Space Administration (NASA) under NSF Cooperative Agreement No. EAR-0735156. Data for the figures in this paper are freely available upon request to L. Liu.

References

Abdalati, W., and K. Steffen (2001), Greenland ice sheet melt extent: 1979–1999, *Journal of Geophysical Research: Atmospheres*, *106*(D24), 33983–33988.

Altamimi, Z., L. Métivier, and X. Collilieux (2012), ITRF2008 plate motion model, *Journal of Geophysical Research: Solid Earth*, *117*, B07402, doi:10.1029/2011JB008930.

Amiri-Simkooei, A. R. (2013) On the nature of GPS draconitic year periodic pattern in multivariate position time series, *Journal of Geophysical Research: Solid Earth*, *118*(5), 2500–2511, doi: 10.1002/jgrb.50199.

Andresen, C. S., K. K. Kjeldsen, B. E. Harden, N. Norgaard-Pedersen, and K. H. Kjær (2014), Outlet glacier dynamics and bathymetry at Upernavik Isstrøm and Upernavik Isfjord, North-West Greenland, *Geological Survey of Denmark and Greenland Bulletin, 31*, 79–82.

Bevan, S. L., A. Luckman, S. A. Khan, and T. Murray (2015), Seasonal dynamic thinning at Helheim Glacier, *Earth and Planetary Science Letters*, *415*(0), 47–53, doi: 10.1016/j.epsl.2015.01.031.

Bevis, M., J. Wahr, S. A. Khan, F. B. Madsen, A. Brown, M. Willis, E. Kendrick, P. Knudsen, J. E. Box, T. van Dam, D. J. Caccamise, B. Johns, T. Nylen, R. Abbott, S. White, J. Miner, R. Forsberg, H. Zhou, J. Wang, T. Wilson, D. Bromwich, and O. Francis (2012),

© 2016 American Geophysical Union. All rights reserved.

Accepted Article

Accepted Article

Bedrock displacements in Greenland manifest ice mass variations, climate cycles and climate change, *Proceedings of the National Academy of Sciences*, *109*(30), 11944–11948, doi:10.1073/pnas.1204664109.

Blewitt, G. (2003), Self-consistency in reference frames, geocenter definition, and surface loading of the solid Earth, *Journal of Geophysical Research: Solid Earth*, *108*(B2), 2103, doi:10.1029/2002JB002082.

Boehm, J., B. Werl, and H. Schuh (2006), Troposphere mapping functions for GPS and very long baseline interferometry from European Centre for Medium-Range Weather Forecasts operational analysis data, *Journal of Geophysical Research: Solid Earth, 111*, B02406. doi: 10.1029/2005JB003629.

Dill, R., V. Klemann, Z. Martinec, and M. Tesauro (2015), Applying local Green's functions to study the influence of the crustal structure on hydrological loading displacements, *Journal of Geodynamics*, *88*(0), 14–22, doi:10.1016/j.jog.2015.04.005.

Dong, D., P. Fang, Y. Bock, M. K. Cheng, and S. Miyazaki (2002), Anatomy of apparent seasonal variations from GPS-derived site position time series, *Journal of Geophysical Research: Solid Earth*, *107*(B4), 9–16, doi:10.1029/2001JB000573.

Dong, D., T. Yunck, and M. Heflin (2003), Origin of the International Terrestrial Reference Frame, *Journal of Geophysical Research: Solid Earth*, *108*(B4), 2200, doi:10.1029/2002JB002035.

Dziewonski, A. and D. Anderson (1981), Preliminary Reference Earth Model (PREM), *Physics of the Earth and Planetary Interiors*, *25*(4), 297–356.

Farrell, W. E. (1972), Deformation of Earth by surface loads, *Reviews of Geophysics and Space Physics*, *10*(3), 761–797.

Fettweis, X., B., Franco, M. Tedesco, J. H. van Angelen, J. T. M., Lenaerts, M. R. van den Broeke, and H. Gallee (2013), Estimating the Greenland ice sheet surface mass balance contribution to future sea level rise using the regional atmospheric climate model MAR, *The Cryosphere, 7*, 469-489, doi:10.5194/tc-7-469-2013.

Fukumori, I. (2002), A partitioned Kalman filter and smoother, *Monthly Weather Review*, *130*(5), 1370–1383.

Grapenthin, R., F. Sigmundsson, H. Geirsson, T. Árnadóttir, and V. Pinel (2006), Icelandic rhythmics: Annual modulation of land elevation and plate spreading by snow load, *Geophysical Research Letters*, 33, L24305, doi:10.1029/2006GL028081.

Hanna, E., P. Huybrechts, J. Cappelen, K. Steffen, R. C. Bales, E. Burgess, J. R. McConnell, J. Peder Steffensen, M. Van den Broeke, and L. Wake (2011), Greenland Ice Sheet surface mass balance 1870 to 2010 based on Twentieth Century Reanalysis, and links with global climate forcing, *Journal of Geophysical Research: Atmospheres*, *116*, D24121 doi:10.1029/2011JD016387.

Jentzsch, G. (1997), Earth tides and ocean tidal loading, in *Tidal Phenomena*, edited by H. Wilhelm, W. Zurn, and H. G. Wenzel, pp. 145–171, Springer.

© 2016 American Geophysical Union. All rights reserved.

Accepted Article

Jiang, Y., T. H. Dixon, and S. Wdowinski (2010), Accelerating uplift in the North Atlantic region as an indicator of ice loss, *Nature Geoscience*, *3*(6), 404–407, doi:10.1038/ngeo845.

Joughin, I., S. B. Das, M. A. King, B. E. Smith, I. M. Howat, and T. Moon (2008), Seasonal speedup along the western flank of the Greenland ice sheet, *Science*, *320*(5877), 781–783, doi: 10.1126/science.1153288.

Kalnay, E., M. Kanamitsu, R. Kistler, W. Collins, D. Deaven, L. Gandin, M. Iredell, S. Saha, G. White, J. Woollen, Y. Zhu, A. Leetmaa, R. Reynolds, M. Chelliah, W. Ebisuzaki, W. Higgins, J. Janowiak, K. C. Mo, C. Ropelewski, J. Wang, R. Jenne, and D. Joseph (1996), The NCEP/NCAR 40-year reanalysis project, *Bulletin of the American Meteorological Society*, *77*(3), 437–471.

Khan, S. A., J. Wahr, L. A. Stearns, G. S. Hamilton, T. van Dam, K. M. Larson, and O. Francis (2007), Elastic uplift in southeast Greenland due to rapid ice mass loss, *Geophysical Research Letters*, *34*(21), L21701, doi:10.1029/2007GL031468.

Khan, S. A., J. Wahr, E. Leuliette, T. van Dam, K. M. Larson, and O. Francis (2008), Geodetic measurements of postglacial adjustments in Greenland, *Journal of Geophysical Research: Solid Earth*, *113*(B2), B02402, doi:10.1029/2007JB004956.

Khan, S. A., L. Liu, J. Wahr, I. Howat, I. Joughin, T. van Dam, and K. Fleming (2010), GPS measurements of crustal uplift near Jakobshavn Isbræ to glacial ice mass loss, *Journal of Geophysical Research*, *115*(B9), B09405, doi:10.1029/2010JB007490.

Khan, S. A., K. H. Kjær, N. J. Korsgaard, J. Wahr, I. R. Joughin, L. H. Timm, J. L. Bamber, M. R. van den Broeke, L. A. Stearns, G. S. Hamilton, B. M. Csatho, K. Nielsen, R. Hurkmans, and G. Babonis (2013), Recurring dynamically induced thinning during 1985 to 2010 on Upernavik Isstrøm, West Greenland, *Journal of Geophysical Research: Earth Surface*, *118*(1), 111–121, doi:10.1029/2012JF002481.

Khan, S. A., I. Sasgen, M. Bevis, T. van Dam, J. L. Bamber, J. Wahr, M. Willis, K. H. Kjær, B. Wouters, V. Helm, B. Csatho, K. Fleming, A. A. Bjørk, A. Aschwanden, P. Knudsen, and P. K. Munneke (2016), Geodetic measurements reveal similarities between post–Last Glacial Maximum and present-day mass loss from the Greenland ice sheet, *Science Advances*, 2(9), doi:10.1126/sciadv.1600931.

Kim, S.-B., T. Lee, and I. Fukumori (2007), Mechanisms controlling the interannual variation of mixed layer temperature averaged over the Niño-3 region, *Journal of Climate*, *20*(15), 3822–3843, doi:10.1175/JCLI4206.1.

Kouba, J. (2008), Implementation and testing of the gridded Vienna Mapping Function 1 (VMF1), *Journal of Geodesy*, *82*(4-5), 193–205, doi:10.1007/s00190-007-0170-0.

Larsen, S. H., S. A. Khan, A. P. Ahlstrøm, C. S. Hvidberg, M. J. Willis, and S. B. Andersen (2016), Increased mass loss and asynchronous behavior of marine-terminating outlet glaciers at Upernavik Isstrøm, NW Greenland, *Journal of Geophysical Research: Earth Surface.*, *121*, doi:10.1002/2015JF003507.

Nielsen, K., S. A. Khan, N. J. Korsgaard, K. H. Kjær, J. Wahr, M. Bevis, L. A. Stearns, and

© 2016 American Geophysical Union. All rights reserved.

Accepted Article

L. H. Timm (2012), Crustal uplift due to ice mass variability on Upernavik Isstrøm, West Greenland, *Earth and Planetary Science Letters*, *353–354*, 182–189, doi:10.1016/j.epsl.2012.08.024.

Noël, B., W. J. van de Berg, E. van Meijgaard, P. Kuipers Munneke, R. S. W. van de Wal, and M. R. van den Broeke (2015), Evaluation of the updated regional climate model RACMO2.3: summer snowfall impact on the Greenland Ice Sheet, *The Cryosphere*, *9*(5), 1831–1844, doi:10.5194/tc-9-1831-2015.

Ray, J., Z. Altamimi, X. Collilieux, and T. van Dam (2008), Anomalous harmonics in the spectra of GPS position estimates, *GPS Solutions*, *12*(1), 55–64, doi:10.1007/s10291-007-0067-7.

Rignot, E., I. Velicogna, M. R. van den Broeke, A. Monaghan, and J. T. M. Lenaerts (2011), Acceleration of the contribution of the Greenland and Antarctic ice sheets to sea level rise, *Geophys. Res. Lett*., 38, L05503, doi:10.1029/2011GL046583.

Rodell, M., P. Houser, U. e. a. Jambor, J. Gottschalck, K. Mitchell, C. Meng, K. Arsenault, B. Cosgrove, J. Radakovich, M. Bosilovich, et al. (2004), The global land data assimilation system, *Bulletin of the American Meteorological Society*, *85*(3), 381–394.

Santamaría-Gómez, A., and A. Mémin (2015), Geodetic secular velocity errors due to interannual surface loading deformation, *Geophysical Journal International*, *202*(2), 763-767, doi:10.1093/gji/ggv190.

Scherneck, H.-G., and M. S. Bos (2002), Ocean tide and atmospheric loading, *in IVS 2002 General Meeting Proceedings, Tsukuba, Japan, February 4-7, 2002*, pp. 205–214, http://holt.oso.chalmers.se/loading (lastly accessed on December 29, 2015).

Sole, A. J., D. W. F. Mair, P. W. Nienow, I. D. Bartholomew, M. A. King, M. J. Burke, and I. Joughin (2011), Seasonal speedup of a Greenland marine-terminating outlet glacier forced by surface melt–induced changes in subglacial hydrology, *Journal of Geophysical Research: Earth Surface*, *116*, F03014, doi: 10.1029/2010JF001948.

van Angelen, J., J. Lenaerts, S. Lhermitte, X. Fettweis, P. Kuipers Munneke, M. Broeke, E. v. Meijgaard, and C. Smeets (2012), Sensitivity of Greenland Ice Sheet surface mass balance to surface albedo parameterization: a study with a regional climate model, *The Cryosphere*, *6*(5), 1175–1186.

van Dam, T. and J. Wahr (1987), Displacements of the Earth’s surface due to atmospheric loading: Effects on gravity and baseline measurements, *Journal of Geophysical Research*, *92*(B2), 1281–1286, doi: 10.1029/JB092iB02p01281.

van den Broeke, M., J. Bamber, J. Ettema, E. Rignot, E. Schrama, W. J. van de Berg, E. van Meijgaard, I. Velicogna, and B. Wouters (2009), Partitioning recent Greenland mass loss, *Science*, *326*(5955), 984–986.

Wahr, J., T. van Dam, K. Larson, and O. Francis (2001), Geodetic measurements in Greenland and their implications, *Journal of Geophysical Research: Solid Earth*, *106*(B8), 16567–16581, doi:10.1029/2001JB000211.

Wahr, J., S. A. Khan, T. Dam, L. Liu, J. H. Angelen, M. R. Broeke, and C. M. Meertens

© 2016 American Geophysical Union. All rights reserved.

(2013), The use of GPS horizontals for loading studies, with applications to northern California and southeast Greenland, *Journal of Geophysical Research: Solid Earth*, 118, 1795–1806.

Wang, H., L. Xiang, L. Jia, L. Jiang, Z. Wang, B. Hu, and P. Gao (2012), Load Love numbers and Green's functions for elastic Earth models PREM, iasp91, ak135, and modified models with refined crustal structure from Crust 2.0, *Computers & Geosciences*, *49*(0), 190–199, doi: 10.1016/j.cageo.2012.06.022.

Williams, S. D. P., Y. Bock, P. Fang, P. Jamason, R. M. Nikolaidis, L. Prawirodirdjo, M. Miller, and D. J. Johnson (2004), Error analysis of continuous GPS position time series, *Journal of Geophysical Research: Solid Earth*, *109*, B03412. doi:10.1029/2003JB002741.

Accepted Article

© 2016 American Geophysical Union. All rights reserved.

Accepted Article

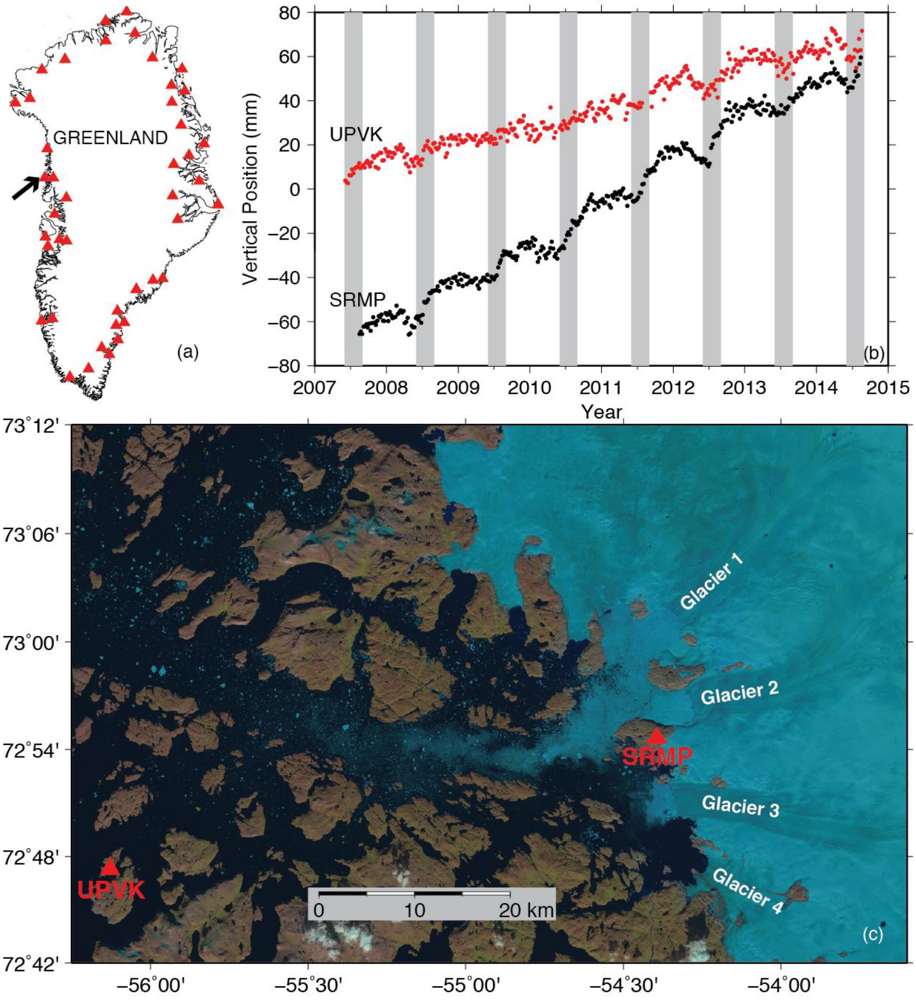

Figure 1. (a) Map of GNET stations (red triangles) around Greenland. The arrow points to the area near Upernavik Isstrøm. (b) Time series of vertical positions measured at GPS stations SRMP (black) and UPVK (red). The gray bars denote June-July-August (JJA) in each year (same in all the time series plots shown in this paper). (c) A Landsat image of Upernavik Isstrøm taken on July 30, 2015. Red triangles mark the location of the two GPS stations. Snow and ice appear in blue.

© 2016 American Geophysical Union. All rights reserved.

Accepted

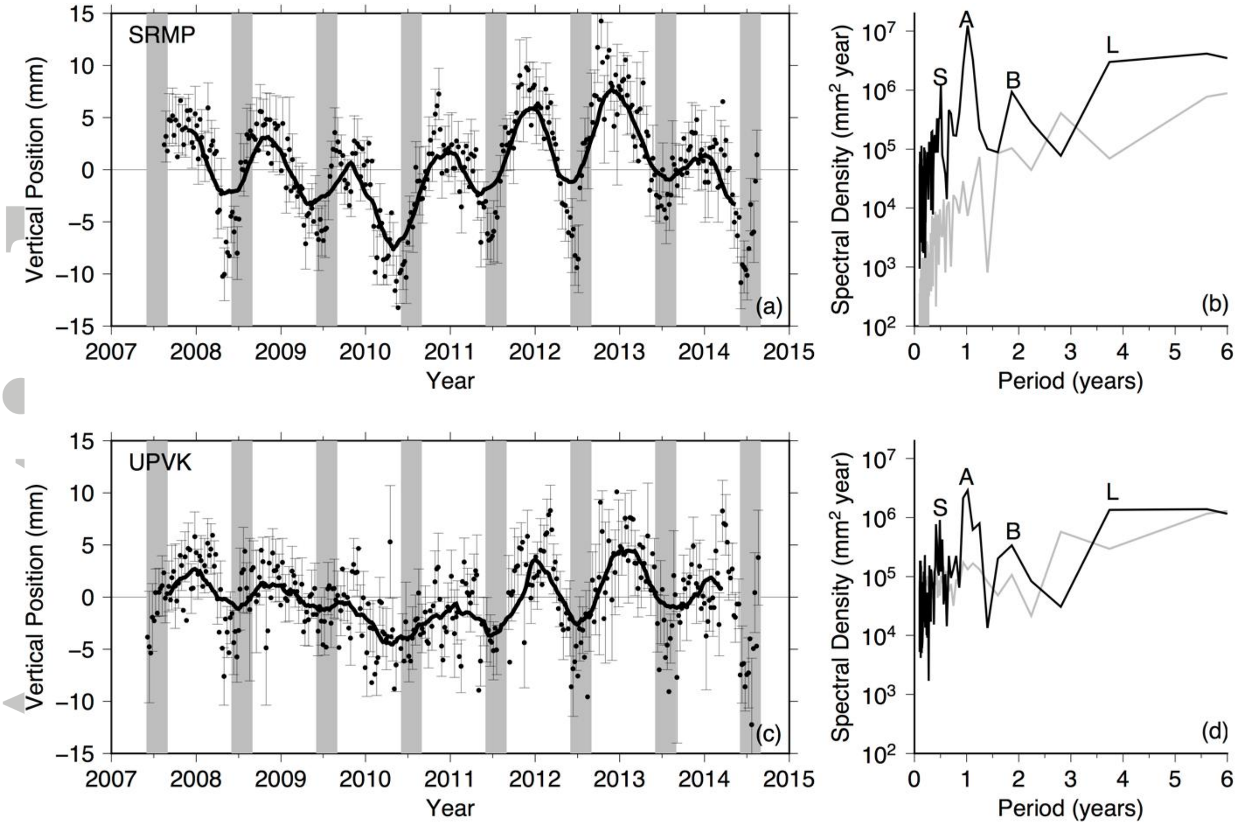

Figure 2. (a) Time series of detrended vertical positions (black dots) at SRMP. For clarity, one-σ uncertainties are shown as error bars at every other GPS solution. The solid line is the smoothed time series after applying a 6-month moving average. (b) Periodogram of the GPS vertical positions at SRMP. 'S', 'A', 'B', and 'L' mark the spectrum peaks at the semi-annual, annual, bi-annual, and longer (~4 years) periods, respectively. The gray line is the periodogram of the GPS errors. (c) and (d) are similar to (a) and (b), respectively, but for the UPVK station.

© 2016 American Geophysical Union. All rights reserved.

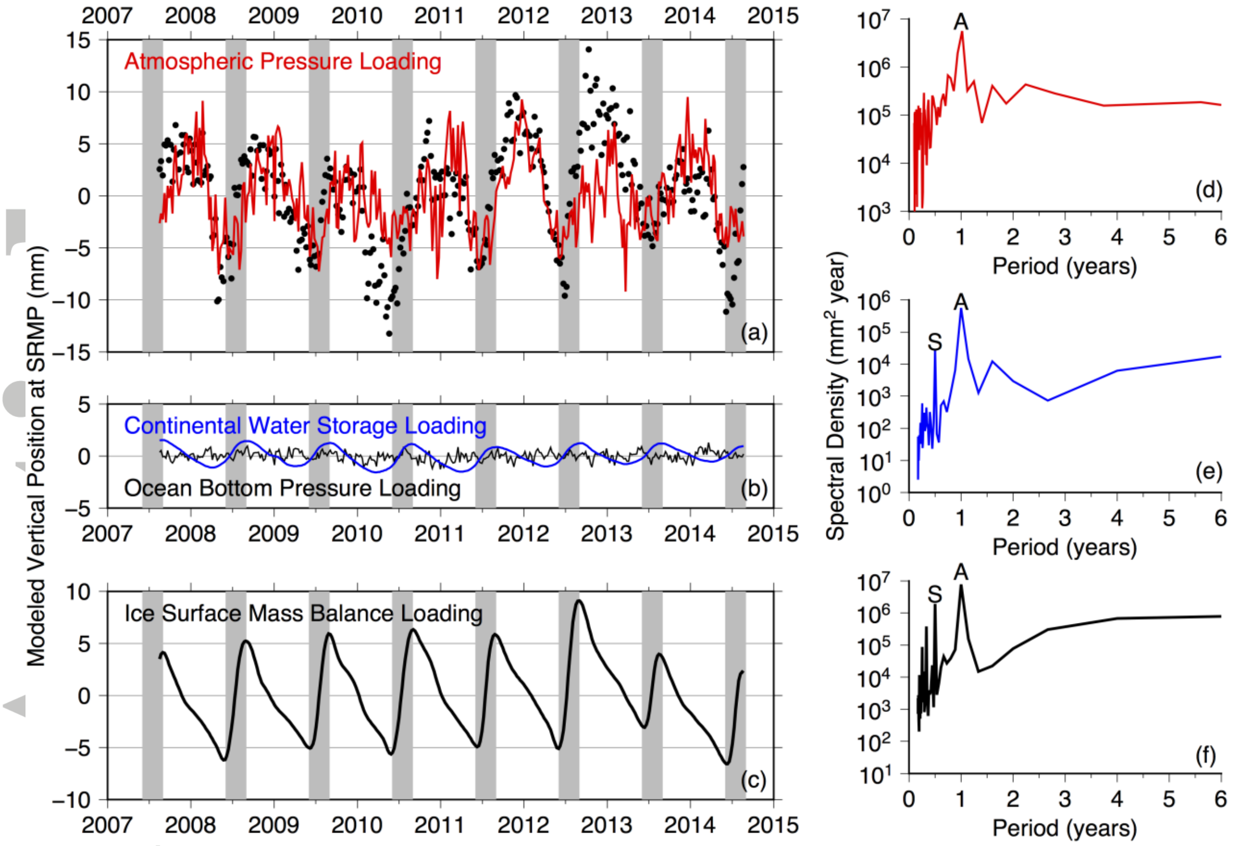

Figure 3. Modeled elastic vertical displacements at SRMP in response to the various loads. All the time series have been detrended. (a) The red line shows the vertical displacements due to atmospheric pressure loading. The black dots are the same GPS data as presented in Figure 2a; they are shown here again to allow for a direct comparison with the modeled displacements. (b) The blue line shows continental water mass loading displacements. The thin black line shows ocean bottom pressure loading displacements. (c) Ice surface mass balance loading displacements. (d), (e), and (f) show the periodograms of the corresponding atmospheric pressure loading, continental water mass loading, and SMB loading, respectively. 'S' and 'A' indicate spectrum peaks at semi-annual and annual periods, respectively.

Accepted

© 2016 American Geophysical Union. All rights reserved.

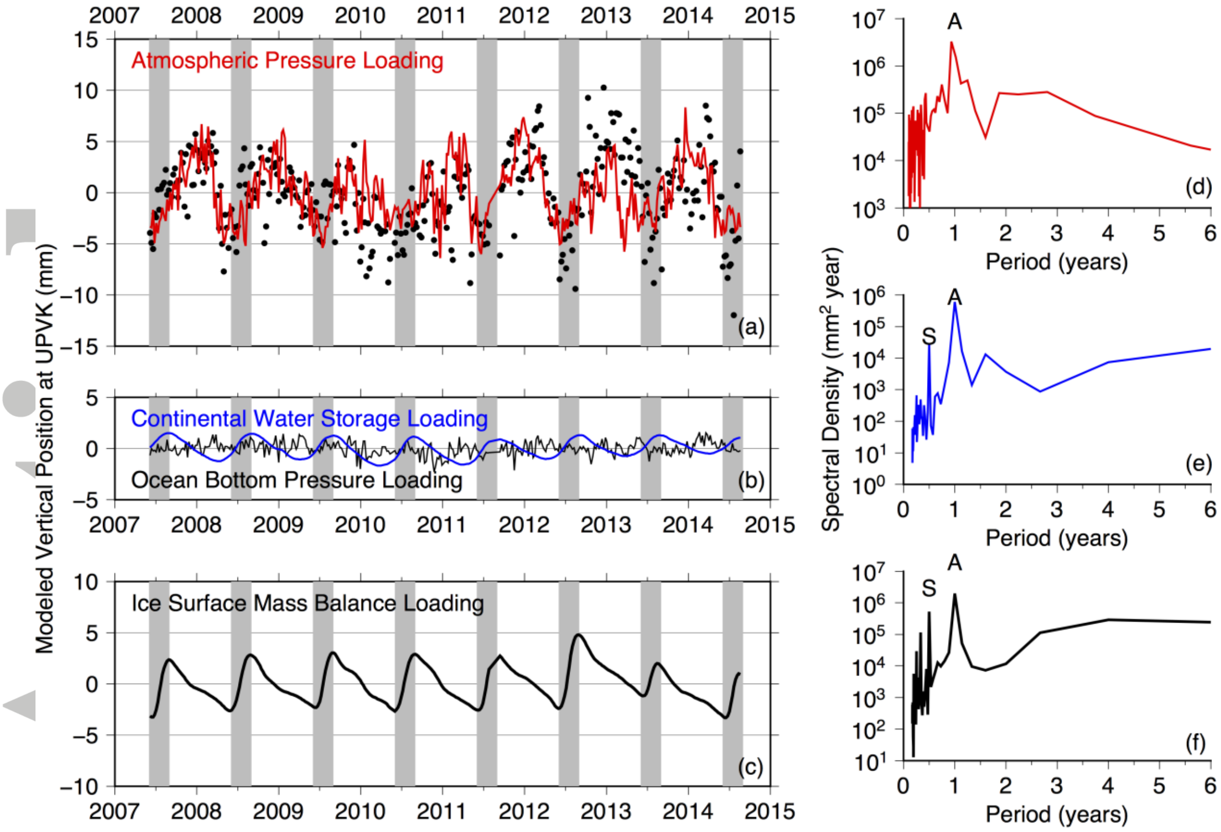

Figure 4. Similar to Figure 3 but for modeled vertical displacements at UPVK in response to various loading sources.

Accepted

© 2016 American Geophysical Union. All rights reserved.

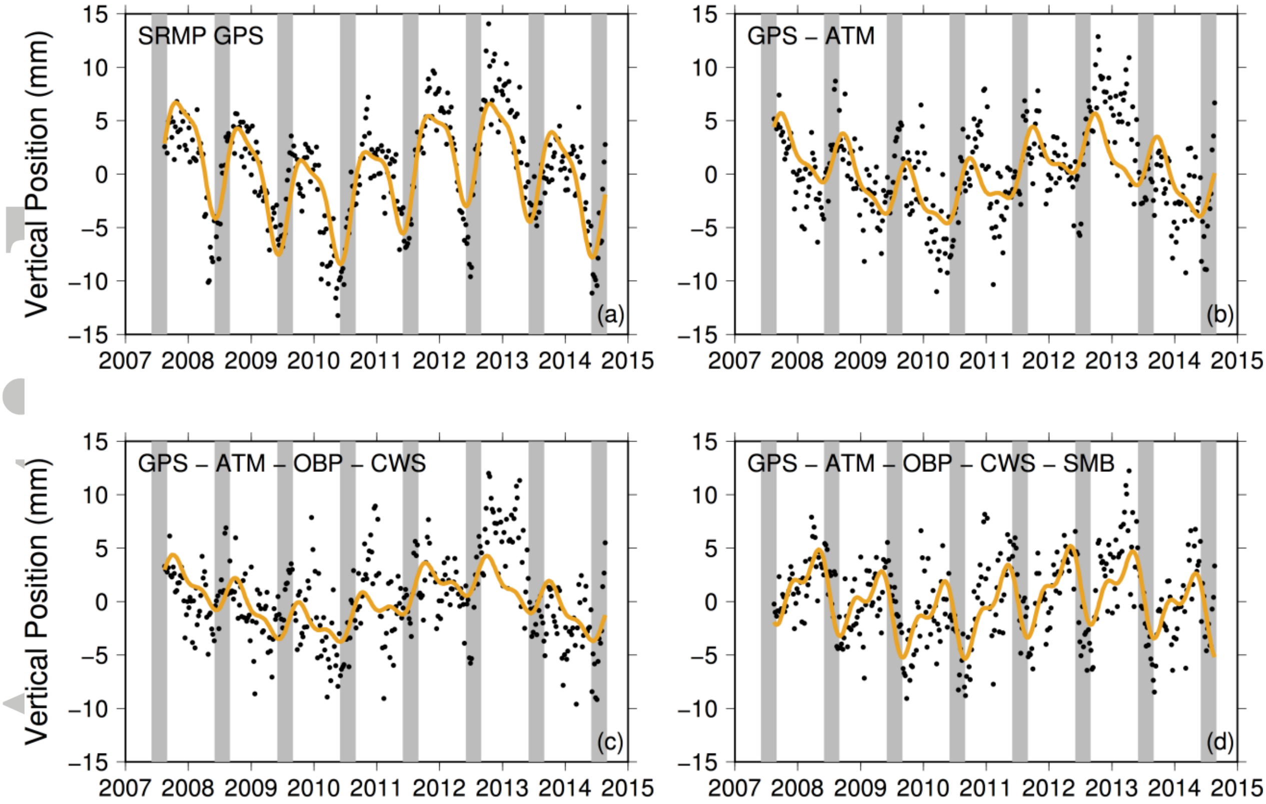

Figure 5. Time series of GPS vertical positions (black dots) after removing the modeled loading displacements at SRMP. (a) shows the same GPS as shown in Figure 2a. The orange line shows the best-fit four-harmonic model using equation (1). (b) shows the residuals after removing the modeled ATM loading. (c) shows the residuals after further removing OBP and CWS. (d) shows the residuals after removing all the modeled surface mass loading components, including the SMB.

Accepted

© 2016 American Geophysical Union. All rights reserved.

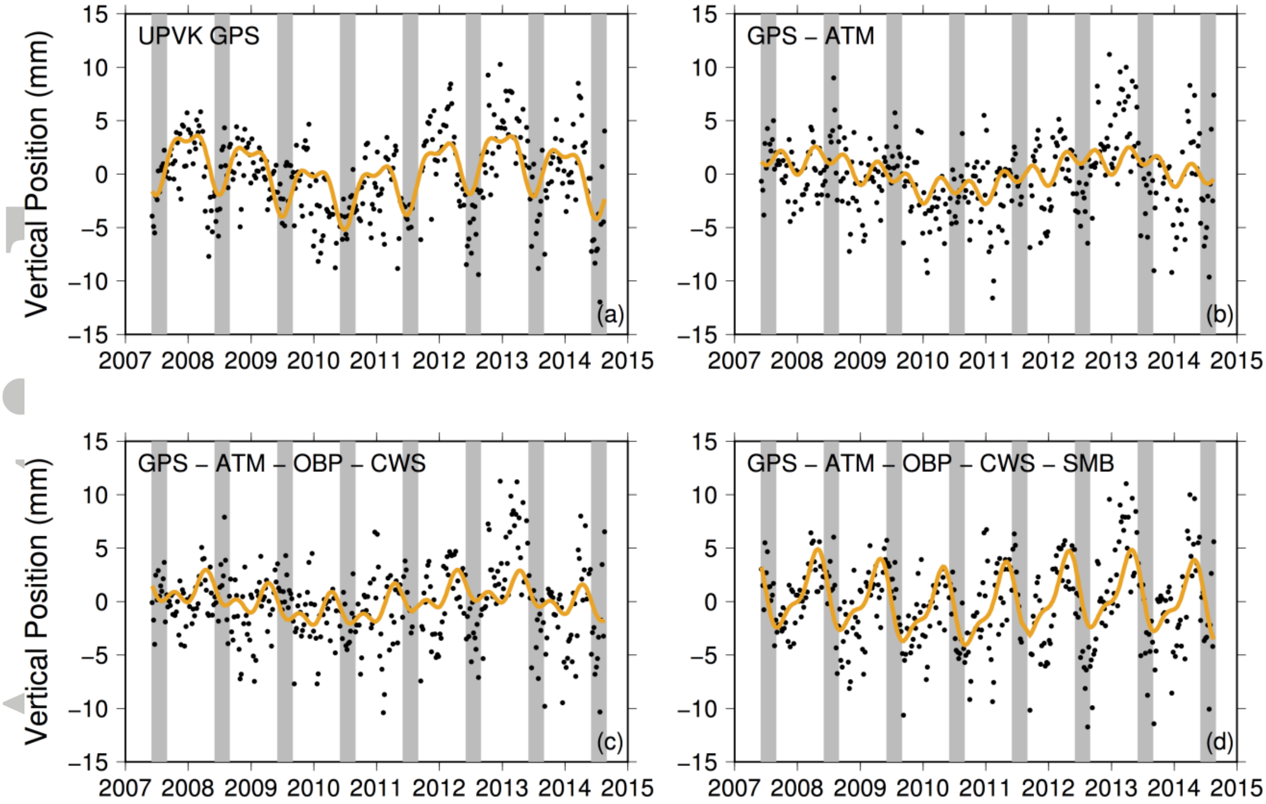

Figure 6. Similar to Figure 5 but for the vertical residuals at UPVK after the modeled loading displacements.

Accepted

© 2016 American Geophysical Union. All rights reserved.

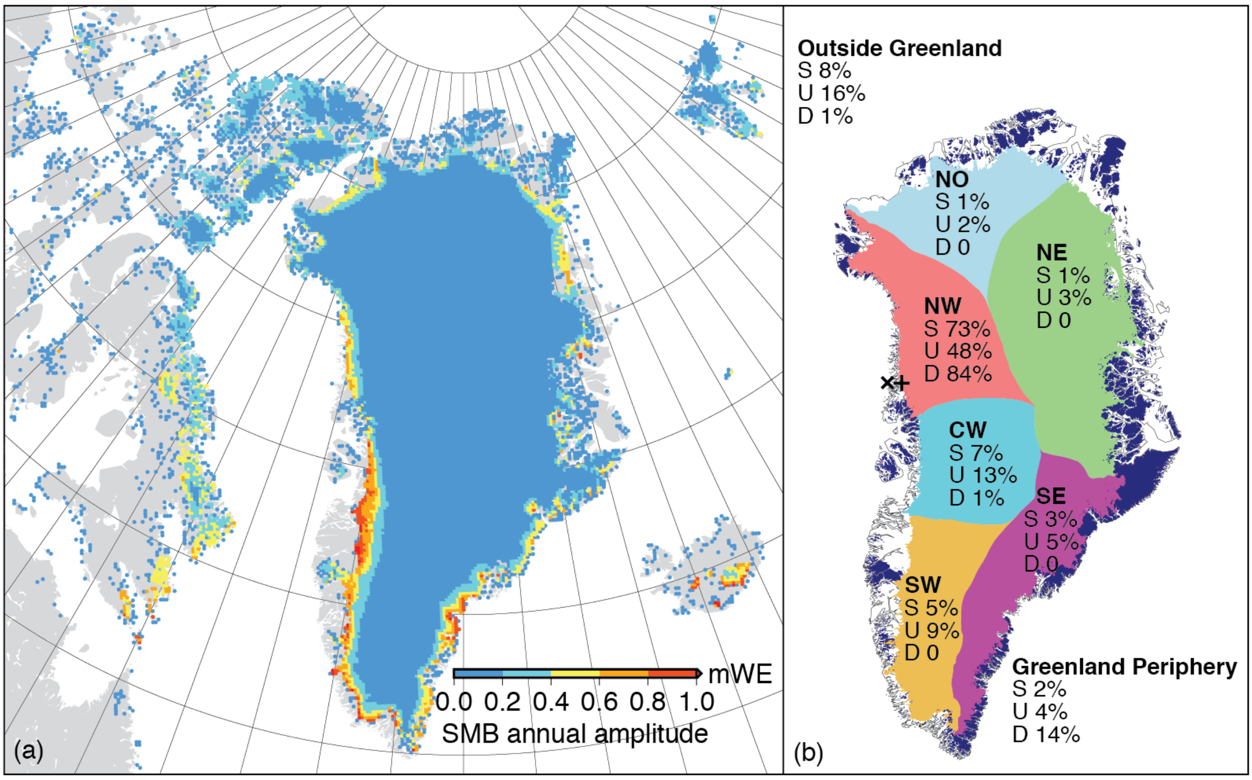

Figure 7. (a) Map of the annual amplitude of SMB (units: meters water equivalent or mWE), obtained from the RACMO2.3 monthly SMB fields from 2007.5 to 2014.7. (b) Map of major drainage basins of Greenland Ice Sheet (labeled as ‘NW’ for northwest, ‘CW’ for central-west, ‘SW’ for southwest, SE’ for southeast, ‘NE’ for northeast, and ‘NO’ for north) and peripheral glaciers in Greenland (dark blue). The plus (+) and cross (×) symbols mark the positions of SRMP and UPVK, respectively. Under each unit label is a list of contributions in percentage from each unit to the annual amplitude of SMB loading displacements at SRMP (‘S’), UPVK (‘U’), and the station difference (‘D’). ‘D 0’ means the contribution to the station difference is smaller than 1% and negligible.

Accepted

© 2016 American Geophysical Union. All rights reserved.

Accepted Article

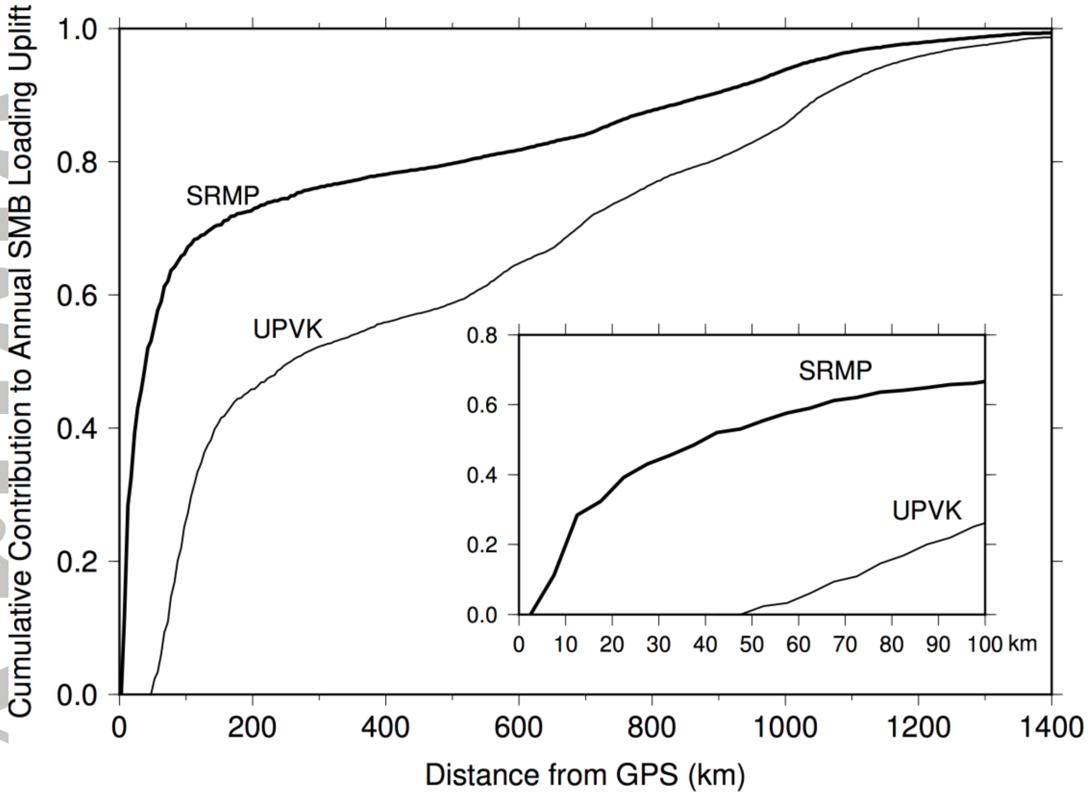

Figure 8. Cumulative contribution to the annual SMB loading uplift at SRMP (thick line) and UPVK (thin line), normalized with the total annual amplitude at each station. The inset shows a zoom-in distance range of 0–100 km.

© 2016 American Geophysical Union. All rights reserved.

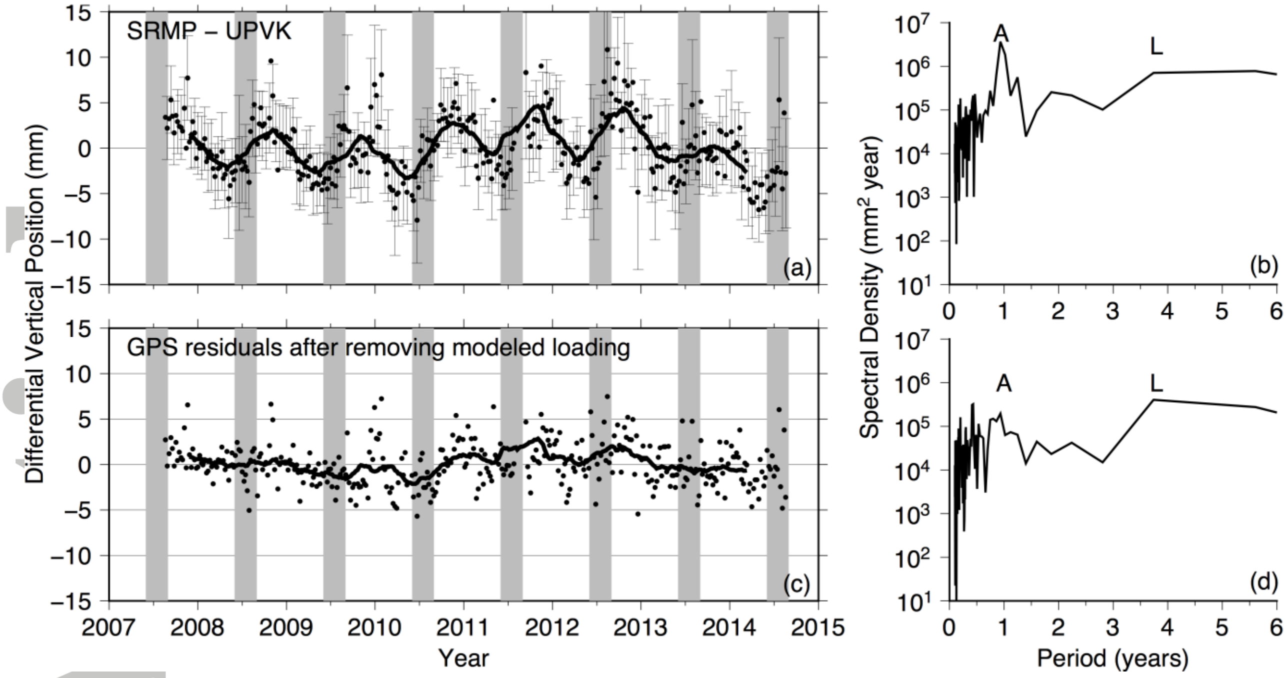

Figure 9. Similar to Figure 2 but for (a) time series of the differences between the detrended vertical positions measured at SRMP and UPVK and (b) its periodogram. (c) time series of the residuals after removing the modeled loading from the difference GPS and (d) its periodogram.

Accepted

© 2016 American Geophysical Union. All rights reserved.

Accepted Article

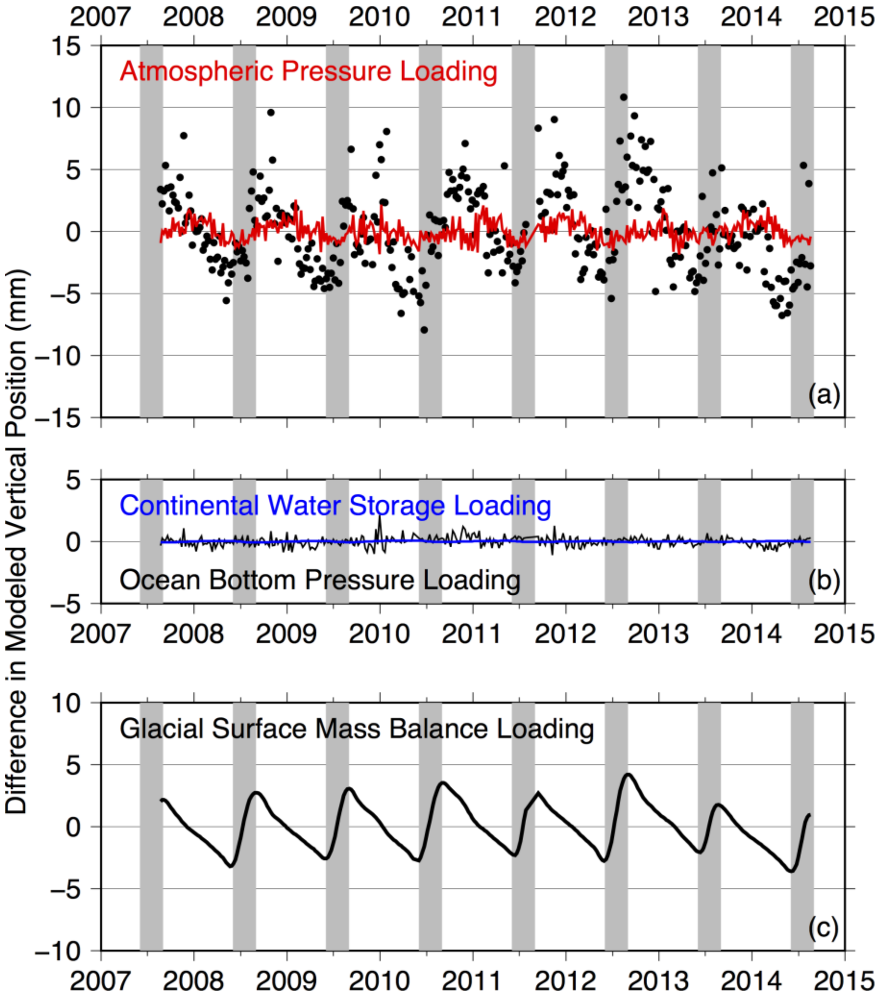

Figure 10. Similar to Figure 3 but for the differences of modeled vertical displacements between SRMP and UPVK

© 2016 American Geophysical Union. All rights reserved.

Accepted Article

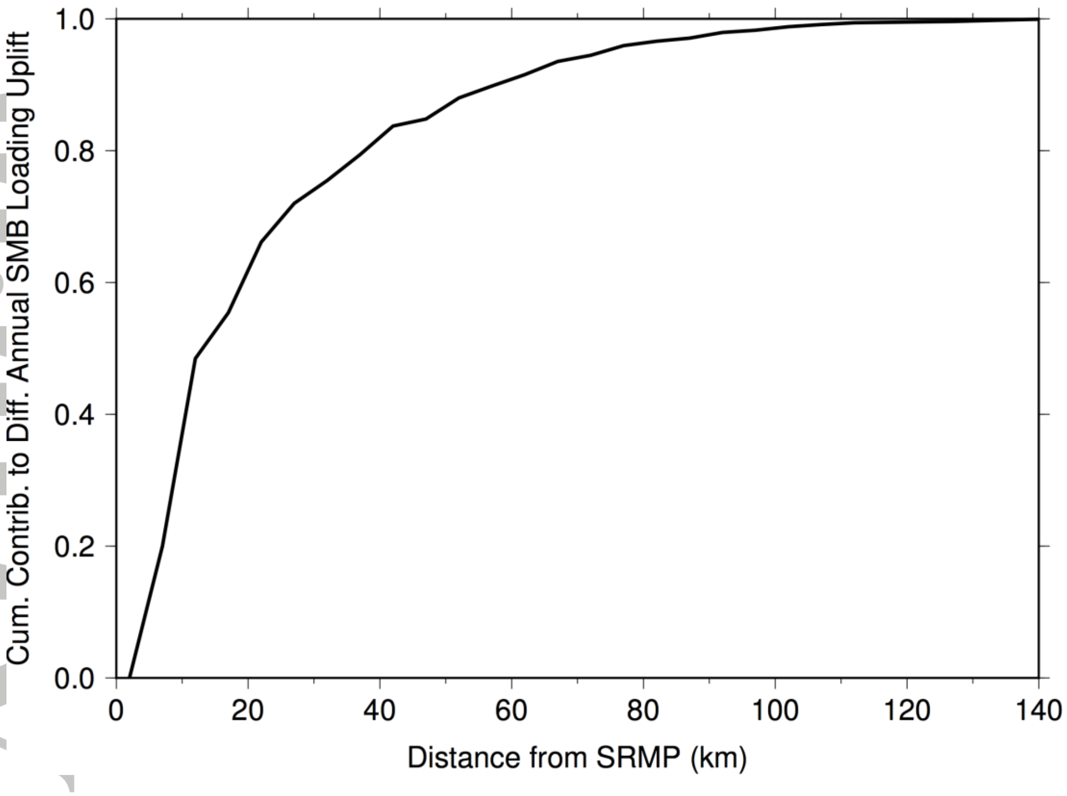

Figure 11. Similar to Figure 8 but for the cumulative contribution to the differential SMB loading uplift between SRMP and UPVK.

© 2016 American Geophysical Union. All rights reserved.

Table 1. Source models of surface mass changes

Surface Mass Component	**Source Model**	**Temporal intervals**	**Grid spacing**	**Spatial extent**
Atmospheric pressure	NCEP	6 hours	2.5° by 2.5°	Global
Ocean bottom pressure	ECCO	12 hours	1° by 1° (except near the equator)	80° S–80° N
Continental water storage	GLDAS-Noah	monthly	1° by 1°	Global, excluding ice sheets and permafrost areas
Ice surface mass balance	RACMO2.3	monthly	~11 km by 11 km	Greenland and surroundings (52.1–87.3° N, 120.85–42.35° E)

Table 2. Annual amplitudes and phases of the GPS data and modeled vertical loading displacements from various surface mass changes. The uncertainties refer to the one-σ root-mean-squares errors. The loading displacements due to ocean bottom pressure changes show little annual changes (smaller than 0.1 mm at SRMP and 0.2 mm at UPVK), which are not included in this table.

Components	SRMP		UPVK	
	Amplitude (mm)	Phase (day of year since January 1)	Amplitude (mm)	Phase (day of year since January 1)
GPS	4.8 ± 0.1	331 ± 2	2.3 ± 0.1	365 ± 3
Atmospheric pressure	3.4 ± 0.1	362 ± 2	2.8 ± 0.1	360 ± 2
Continental water storage	1.1 ± 0.1	258 ± 1	1.1 ± 0.1	257 ± 1
Ice surface mass balance	4.3 ± 0.3	284 ± 4	2.0 ± 0.2	283 ± 4

Accepted Article

© 2016 American Geophysical Union. All rights reserved.

Accepted Article

Table 3. Best-fit amplitude and phase of annual cycles after the sequential steps: (1) removing the atmospheric pressure (ATM) loading displacements, (2) removing the loading displacements from ocean bottom pressure (OBP) and continental water storage (CWS) combined, and (3) removing the SMB loading displacements. The 'GPS' row is the same as listed in Table 2.

	SRMP		UPVK	
	Amplitude (mm)	Phase (day of year since January 1)	Amplitude (mm)	Phase (day of year since January 1)
GPS	4.8 ± 0.1	331 ± 2	2.3 ± 0.1	365 ± 3
After removing ATM	2.6 ± 0.1	287 ± 3	0.5 ± 0.1	158 ± 10
After further removing OBP and CWS	1.8 ± 0.1	309 ± 3	1.2 ± 0.1	94 ± 5
After further removing SMB	2.7 ± 0.1	85 ± 2	3.2 ± 0.1	99 ± 2

Table 4. Ratios of WRMS reduction in vertical position time series, after removing individual loading sources. Columns 'Long-period' and 'Short-period' list the ratios calculated using the components at longer and shorter than the semi-annual period, respectively.

	Ratio of WRMS reduction at SRMP (%)		Ratio of WRMS reduction at UPVK (%)	
	Long-period	Short-period	Long-period	Short-period
ATM removed	26	-14	21	-6
OBP removed	-0.6	2	3	3
CWS removed	4	0.1	-5	0
SMB removed	24	0.7	-4	0.9
All removed	41	-16	-3	-6

© 2016 American Geophysical Union. All rights reserved.

Accepted Article

Table 5. Similar to Table 2 but for the differential verticals between SRMP and UPVK. We exclude the differential ocean bottom pressure and continental water storage loading displacements as their annual changes are smaller than 0.1 mm.

Components	SRMP minus UPVK	
	Amplitude (mm)	Phase (day of year since January 1)
GPS	3.1 ± 0.2	303 ± 3
Atmospheric pressure	0.6 ± 0.1	2 ± 3
Ice surface mass balance	2.2 ± 0.1	286 ± 1

Table 6. Similar to Table 3 but for the differential vertical displacements between SRMP and UPVK

	SRMP minus UPVK	
	Amplitude (mm)	Phase (day of year since January 1)
GPS	3.1 ± 0.2	304 ± 3
After removing ATM	2.9 ± 0.2	293 ± 3
After further removing OBP and CWS	2.8 ± 0.2	295 ± 3
After further removing SMB	0.7 ± 0.2	321 ± 11

© 2016 American Geophysical Union. All rights reserved.

Table 7. Similar to Table 4 but for the differential vertical displacements between SRMP and UPVK. The differential CWS loading displacements are nearly zero and therefore not included in the table.

	Ratio of WRMS reduction (%)	
	Long-periods	Short-periods
ATM removed	4	3
OBP removed	3	0.2
SMB removed	47	-0.5
All removed	55	2

Accepted Article

© 2016 American Geophysical Union. All rights reserved.